

Polyhedral iridaborane chemistry: Elements of the 10-vertex
closo–isonido–isocloso continuum
Molecular structures of [(PPh₃)₂HIrB₉H₉(PPh₃)],
[(PPh₃)(Ph₂PC₆H₄)IrB₉H₇(PPh₃)],
[(PPh₃)(Ph₂PC₆H₄)HIrB₉H₆Cl(PPh₃)],
[(PPh₃)(Ph₂PC₆H₄)HIrB₉H₆(PPh₃)₂] and [(PPh₃)(Ph₂PC₆H₄)HIrB₉H₁₂][☆]

Jonathan Bould^a, William Clegg^{b,c}, John D. Kennedy^{a,*}

^a School of Chemistry, University of Leeds, Leeds LS2 9JT, Northern England, UK

^b School of Natural Sciences (Chemistry), University of Newcastle, Newcastle upon Tyne NE1 7RU, Northern England, UK

^c Daresbury Laboratory, Daresbury, Warrington, Cheshire WA4 4AD, Northern England, UK

Received 25 November 2005; received in revised form 30 January 2006; accepted 30 January 2006

Available online 20 March 2006

It is a pleasure to be able to contribute to this special edition for Mike Mingos in order to recognise his many stimulating experimental and theoretical contributions to many aspects of chemical science.

Abstract

There is experimental difficulty in the isolation and structural definition of examples of compounds of the *isonido* 10-vertex cluster structure in order that they may be added to the pattern of behaviour associated with the 10-vertex *closo–isonido–isocloso* structural continuum in boron-containing cluster chemistry. By contrast, the *closo* and *isocloso* extremes are well recognised, with several definitive examples. An approach involving the synergic application of crystallography (using single-crystal X-ray diffraction analysis and HYDEX), multi-element NMR spectroscopy, and DFT calculations of structure and nuclear magnetic shielding, has been used to delineate and define two basic variants in the quadrilaterally open-faced 10-vertex '*isonido*' {IrB₉} metallaborane system. Type A variants, as in [7,7,7-(PPh₃)₂H-μ-3,7-H-*isonido*-7-IrB₉H₈-9-(PPh₃)] (**2**), have an Ir–H–B bridging hydrogen atom involving a boron atom off the open face, and an Ir–H non-bridging linkage. Type B variants, as in [8-Cl-7-(PPh₃)-μ-7^P,10^C-(Ph₂P-*ortho*-C₆H₄)-*isonido*-7-IrB₉H₆-9-(PPh₃)] (**5**), have no cluster-bridging hydrogen atoms and no Ir–H unit. Previously unreported single-crystal X-ray diffraction analyses are given for *isonido* type-A [7-(PPh₃)-μ-7^P,10^C-(Ph₂P-*ortho*-C₆H₄)-7-H-μ-3,7-H-*isonido*-7-IrB₉H₈-9-(PPh₃)] (**10**), classical *closo* [7-(PPh₃)-μ-7^P,10^C-(Ph₂P-*ortho*-C₆H₄)-7-H-*closo*-7-IrB₉H₆-3,9-(PPh₃)₂] (**13**) and classical *nido* [6-(PPh₃)-μ-6^P,5^C-(Ph₂P-*ortho*-C₆H₄)-6-H-*nido*-6-IrB₉H₁₂] (**15**). Overall, the work well demonstrates the synergic usage of NMR spectroscopy, single-crystal X-ray crystallography (including HYDEX calculations) and DFT calculations of structure and nuclear shielding, to resolve ambiguous problems of chemical constitution in polyhedral boron-containing cluster chemistry, an approach that should have wider applicability.

© 2006 Elsevier B.V. All rights reserved.

Keywords: Borane cluster; X-ray structure; Metallaboranes; DFT calculations; ¹¹B nuclear shielding; 10-vertex *isonido* cluster types; Polyhedral structural continuum

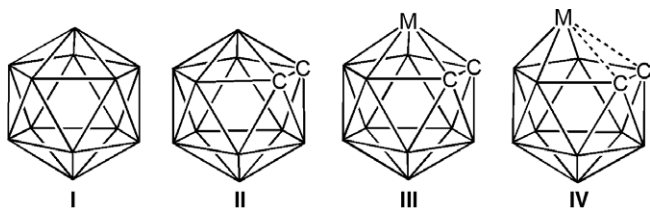
[☆] This article was freely submitted for publication without royalty. By acceptance of this paper, the publisher and/or recipient acknowledges the right of the authors to retain non-exclusive, royalty-free license in and to any copyright covering this paper, along with the right to reproduce all or part of the copyrighted paper.

* Corresponding author.

E-mail address: johnk@chem.leeds.ac.uk (J.D. Kennedy).

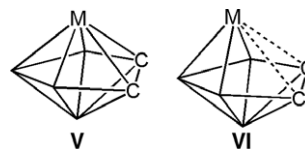
1. Introduction

In the early 1970s Mike Mingos and others developed rules that governed the relationships between the shapes and sizes of clusters of atoms and the numbers of electrons associated with the intracuster bonding [1–8]. A key cluster shape was the 12-vertex icosahedron – as represented by the regular icosahedral $\{B_{12}\}$ framework of the $[closo-B_{12}H_{12}]^{2-}$ anion (schematic I) and by the shapes of its closely related congeners, such as neutral $[closo-1,2-C_2B_{10}H_{12}]$ (schematic II), of which the exact geometry deviates from regular icosahedral principally because of the smaller sizes of the carbon versus the boron atoms. Transition-element centres that can be regarded as making three-orbital two-electron contributions to cluster bonding that mimic the contribution of a $\{BH\}$ cluster vertex, such as $\{Co(\eta^5-C_5H_5)\}$ and $\{Ru(\eta^6-C_6H_6)\}$, can also figure as cluster components [1–6], and so species such as $[(\eta^5-C_5H_5)CoC_2B_9H_{11}]$ and $[(\eta^6-C_6H_6)RuC_2B_9H_{11}]$ also exhibit triangular-faced icosahedral cluster geometries (schematic cluster structure III) [9–11]. These deviate from the regular icosahedral of $[B_{12}H_{12}]^{2-}$ because of the larger sizes of the metal atoms as well as the smaller sizes of the carbon atoms. It was however known since the late 1960s that the incorporation of later-transition-element centres can produce structures that are more open than that of a triangular-faced icosahedron [12–18]. These deviate from icosahedral in that the metal-to-carbon distances now are much longer, and can be regarded as being beyond a range associated with strong intracuster bonding interaction (schematic cluster structure IV). Such ‘slipped *closo*’ species have received detailed analysis from Mike Mingos and co-workers [16,17]. In simplistic terms the ‘slippage’ of cluster opening arises because these types of metal centre have a tendency to bind to the remainder of the cluster principally by the use of two orbitals rather than the three utilized by units such as $\{BH\}$, $\{CH\}$, $\{Co(\eta^5-C_5H_5)\}$, $\{Ru(\eta^6-C_6H_6)\}$ etc., and the metal-to-cluster bonding connectivity is correspondingly diminished.

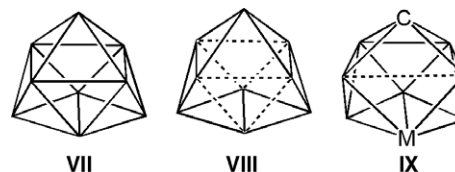


Similar ‘slipped *closo*’ distortions occur in smaller clusters, and in particular in this context studies have been made on seven-vertex $\{PtC_2B_4\}$ systems [18,19], in which again there is slippage away from conventional *closo* (schematic cluster structure V) with longer metal-to carbon interatomic distances (schematic cluster structure VI). The cluster openings observed in these 12-vertex and seven-vertex species are examples of ‘skeletal disobedience’, in that the geometric structures in question do not conform to the straightforward *closo/nido/arachno* geometrical par-

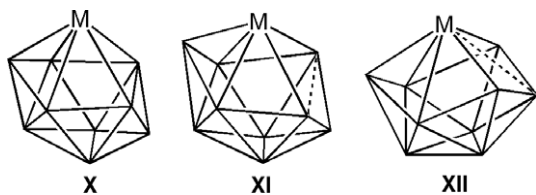
adigm [1–8], and in that they exhibit a cluster opening from pure deltahedral *closo* that may be regarded as anomalous [20].



A different, perhaps more subtle, type of skeletal disobedience has over the years become increasingly manifest [20]. It is apparent that some deltahedral structural motifs are quite flexible. In such clusters, changes of cluster constituents and substituents can often change one or more connectivity distances to such an extent that more open geometries result, often with a quadrilateral open face if only one connectivity is stretched. Alternatively, some clusters may instead be regarded as ‘fragile’ rather than ‘flexible’, in that changes of cluster constituents and substituents can produce catastrophic changes to give another distinct geometric and electronic cluster type. Sometimes the differences between ‘cluster fragility’ and ‘cluster flexibility’ may be difficult to distinguish experimentally. The origins of these sorts of distortion are not yet as clear as the origins of the types of distortion induced by transition-element centres in the ‘slipped *closo*’ cases mentioned above. Examples here include the nine-vertex *closo* system based on the classical tricapped trigonal prismatic motif (schematic cluster structure VII). The basic *closo* $[B_9H_9]^{2-}$ cluster structure is characterised by three somewhat longer (and thence probably weaker) interboron linkages between the three boron atoms constituting each of the two triangular ends of the underlying trigonal prism (hatched lines in schematic cluster structure VIII) [21]. In a number of species, such as, for example, $[(CO)(PPh_3)_2IrCB_7H_8]$ (schematic cluster structure IX) [22,23], the influence of the heteroatoms is to stretch one or more of these longer connectivities towards a separation that can be regarded as non-bonding, giving a quadrilateral open face in a geometry that has been dubbed ‘*isonido*’.



We have long been interested in this last type of stretching phenomenon in the 10-vertex system [24], particularly the stretching of the closed 10-vertex D_{4d} bicapped square antiprismatic geometry X of ostensibly *closo* $\{IrB_9\}$ species to give so-called ‘*isonido*’ 10-vertex geometries XI. A geometrical continuation of this distortion results in a diamond-square-diamond process and the generation of a so-called ‘*isocloso*’ architecture as in schematic XII.

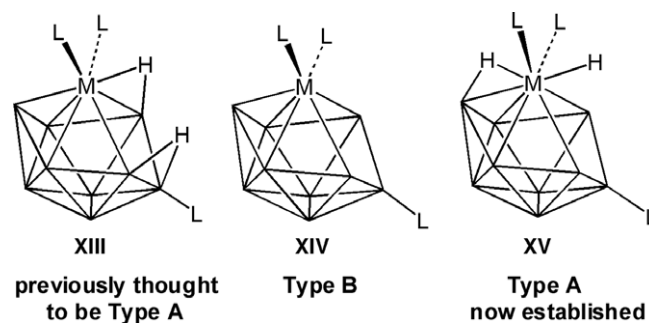


A comprehensive investigation of these latter 10-vertex systems is severely inhibited by the dearth of intermediate ‘*isonido*’ examples and the experimental difficulty of generating such suitable examples. In the original work on the $\{\text{IrB}_9\}$ 10-vertex system, there seemed to be two classes of species within the intermediate *isonido* area **XI** of the structural continuum [24]. Both had quadrilateral open faces. One type, variant A, appeared to have two bridging hydrogen atoms associated with the open face, although there was some uncertainty about their precise positioning (schematic cluster structure **XIII** below). The other type, variant B, had none (schematic cluster structure **XIV** below). In many cases, however, and although it was reasonably certain that the crystallographically determined structures matched solution-phase NMR measurements, because of the low yields, possibilities of lack of robustness in solution, and possibilities of isomerization upon crystallisation, allied with non-ideal crystallographic data sets that precluded hydrogen-atom location, some doubt remained. We now present results from further crystallographic structural work, allied with DFT calculations of structure and ^{11}B nuclear shielding, which clarify the characteristics of these two 10-vertex *isonido* variants A and B. The results presented well exemplify the efficacy of the synergic use of crystallography, NMR spectroscopy and DFT calculations of structure and nuclear shielding to elucidate problems of structure and constitution in polyhedral boron-containing cluster chemistry, and will have general applicability.

2. Results and discussion

Among the 10-vertex $\{\text{IrB}_9\}$ *isonido*-structured cluster compounds just mentioned in Section 1 was one for which we proposed the constitution $[\text{7,7,7-(PPh}_3)_2\text{-}\mu\text{-7,10-H-}\mu\text{-8,9-H-isonido-7-IrB}_9\text{H}_8\text{-9-(PPh}_3)]$ (compound **2**) (note that, for convenience of comparison, in this present paper we use the compound numbering of our previous report [24] for compounds mentioned in both works; compounds newly mentioned in this present work are numbered from **10** onwards). Compound **2** was of variant Type A. Single-crystal X-ray diffraction data were sufficient to give the heavier atom skeletal structure, but were of insufficient quality for hydrogen-atom location. However, NMR spectroscopy showed seven $\{\text{BH}(\textit{exo})\}$ proton resonances, and also two proton resonances for two hydrogen atoms at higher shielding, $\delta(^1\text{H})$ -4.37 and -8.70 ppm. We proposed that these latter two be associated with the open face, one lower field in a BHB bridge, and the one at higher shielding in an IrHB bridge, as they were in typical ranges

associated with those environments (schematic cluster structure **XIII**). The incidence of these two hydrogen atoms contrasted to the constitution of $[\text{8-Cl-7-(PPh}_3)\text{-}\mu\text{-7}^{\text{P}},\text{10}^{\text{C}}\text{-}(\text{Ph}_2\text{P-ortho-C}_6\text{H}_4)\text{-isonido-7-IrB}_9\text{H}_6\text{-9-(PPh}_3)]$ (compound **5**), which does not have two such hydrogen atoms (schematic cluster structure **XIV**). Again, as with compound **2** above, hydrogen atoms were not locatable from the single-crystal X-ray diffraction work on what we then thought to be a crystal of compound **5**, but the crystallographically determined heavier-atom structure did show *isonido* geometry, with its characteristic quadrilateral open face (schematic **XI** above), and NMR spectroscopy revealed *exo*-terminal hydrogen atoms on the six boron atoms that were not otherwise substituted. The detailed dimensions of the basic $\{\text{IrB}_9\}$ skeletal structures of **2** and **5** were apparently very similar indeed. Now, however, there was no NMR evidence for any other cluster hydrogen atoms, bridging or otherwise, in compound **5**. The possibility of any fluxionality among any such hydrogen atoms, resulting in the broadening of their resonances, and thence making them difficult to detect at particular temperatures, was discounted by variable-temperature NMR work.



In view of this difference of two in hydrogen-atom content between compounds **2** and **5** (structural variants A and B, respectively), it was of interest that the two compounds appeared to have such very similar basic cluster geometries. We have therefore now used DFT calculations of structure, and of magnetic shielding of nuclei, to establish and confirm the precise nature of the differences, and thence also to clear previous uncertainties about the constitutions of $[(\text{PPh}_3)_2\text{-HIrB}_9\text{H}_{10}(\text{PPh}_3)]$ (**2**) and $[(\text{PPh}_3)(\text{Ph}_2\text{PC}_6\text{H}_4)\text{IrB}_9\text{H}_6(\text{PPh}_3)]$ (**5**), and thereby better define the Type A and Type B characteristics. DFT calculations at the B3LYP level of theory were employed, using the 6-31G* basis-sets for phosphorus, carbon, boron and hydrogen, and the LANL2DZ basis-set for iridium. The overall analysis is assisted by an X-ray crystallographic data collection on a new species, a Type-A variant, $[\text{7-(PPh}_3)\text{-}\mu\text{-7}^{\text{P}},\text{10}^{\text{C}}\text{-}(\text{Ph}_2\text{P-ortho-C}_6\text{H}_4)\text{-7-H-}\mu\text{-3,7-H-isonido-7-IrB}_9\text{H}_8\text{-9-(PPh}_3)]$ (**10**), in which, now, all cluster hydrogen atoms are located (see Fig. 1, left).

To reduce calculation time, $[(\text{PPh}_3)_2\text{IrB}_9\text{H}_{10}(\text{PPh}_3)]$ (compound **2**) was modelled with PMe_3 ligands rather than PPh_3 , viz., as $[(\text{PMe}_3)_2\text{IrB}_9\text{H}_{10}(\text{PMe}_3)]$ (compound **2a**). As with the other DFT structural calculations reported in this paper, compound **2** was modelled initially using hydrogen

atoms rather than phenyl groups on the phosphine ligands (species **2b**), and then, based on the geometries so obtained, the structural and boron nuclear shielding calculations were extended to the final P-methyl model **2a**. Initial calculations on **2a** did not minimise in accord with our original supposition of two bridging hydrogen atoms associated with a quadrilateral open face (schematic cluster structure **XIII**). However, a stable geometry was achieved with a placement of one hydrogen atom in an Ir–H non-bridging linkage held in a quasi-*endo* configuration above the open

face and the other hydrogen atom in an IrHB bridging position, but involving a boron atom B(3) off the {Ir(7)B(8)B(9)B(10)} open face (Fig. 1, right, and schematic cluster structure **XV**). General non-organyl dimensions for **2a** were very similar to those found experimentally for **2** (Table 1), indicating that the use of the P-methyl variant **2a** as a model for **2** was satisfactory.

An off-open-face bridging hydrogen atom is very rare in boron-containing cluster chemistry, particularly in open-faced species, for which the general incidence for a bridging

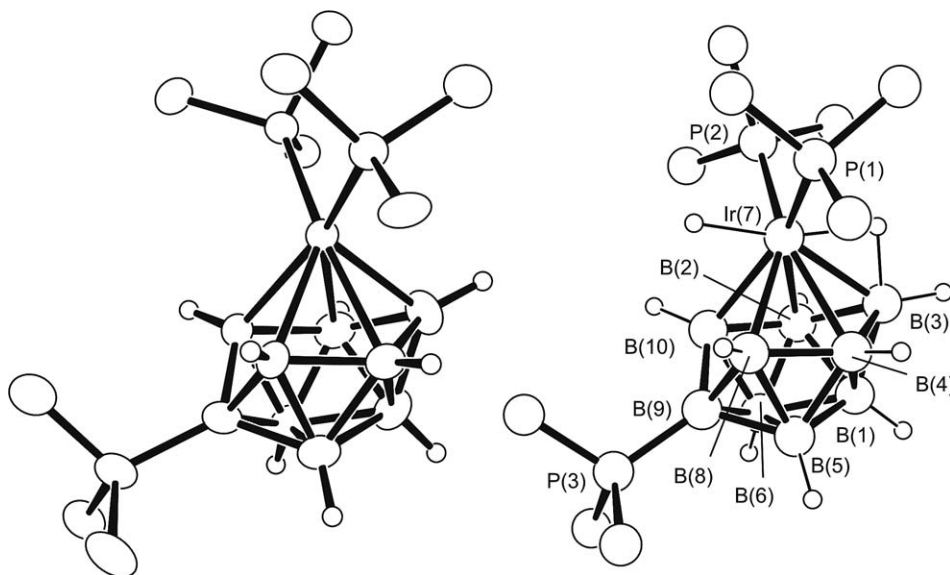


Fig. 1. ORTEP-3 drawings [60] of (left-hand diagram) the crystallographically determined molecular structure of [7,7-(PPh₃)₂-7-H-μ-3,7-H-isonido-7-IrB₉H₈-9-(PPh₃)] (compound **2**) and (right-hand diagram) the DFT-calculated molecular structure of its methyl-for-phenyl analogue [7,7-(PMe₃)₂-7-H-μ-3,7-H-isonido-7-IrB₉H₈-9-(PMe₃)] (**2a**), used to model compound **2** in DFT calculations. For clarity methyl hydrogen atoms are omitted. Selected interatomic dimensions are given in Table 1.

Table 1
Selected measured interatomic separations within compounds **2**, **10**, and **13**, together with calculated interatomic separations within the P-methyl models **2a**, **5a**, **10a** and **13a**, and within the P-hydryl models (see text) **2b**, **12a**, **12b**, **10b** and **13b**^a

Compounds								
	2	2a [2b]	10	10a [10b]	{ 5a }	12b [12c]	13	13a [13b]
Ir(7)–B(2)	2.359(12)	2.369 [2.360]	2.338(3)	2.382 [2.367]	{2.377}	2.374 [2.360]	2.305(4)	2.341 [2.371]
Ir(7)–B(3)	2.193(11)	2.255 [2.260]	2.161(4)	2.236 [2.244]	{2.074}	2.069 [2.073]	2.099(4)	2.099 [2.081]
Ir(7)–B(4)	2.343(12)	2.386 [2.360]	2.363(4)	2.378 [2.358]	{2.360}	2.369 [2.365]	2.324(4)	2.379 [2.359]
Ir(7)–B(8)	2.320(11)	2.330 [2.318]	2.306(4)	2.339 [2.334]	{2.196}	2.239 [2.239]	2.286(4)	2.330 [2.334]
Ir(7)–B(10)	2.304(11)	2.341 [2.318]	2.275(4)	2.311 [2.297]	{2.302}	2.291 [2.277]	2.307(5)	2.336 [2.325]
Ir(7)–B(9)	3.319	3.320 [3.268]	3.265	3.240 [3.199]	{3.125}	3.104 [3.048]	3.429	3.414 [3.374]
B(8)–B(10)	2.158(13)	2.223 [2.271]	2.266	2.354 [2.384]	{2.392}	2.442 [2.495]	1.992(6)	2.069 [2.114]
B(8)–B(9)	1.646(16)	1.693 [1.692]	1.704(5)	1.706 [1.702]	{1.706}	1.710 [1.708]	1.712(6)	1.700 [1.687]
B(9)–B(10)	1.684(14)	1.689 [1.692]	1.714(5)	1.710 [1.706]	{1.712}	1.710 [1.706]	1.706(6)	1.690 [1.696]
B(5)–B(9)	1.678(16)	1.694 [1.694]	1.709(5)	1.711 [1.706]	{1.736}	1.729 [1.727]	1.702(6)	1.684 [1.679]
B(6)–B(9)	1.709(15)	1.697 [1.694]	1.707(5)	1.708 [1.703]	{1.723}	1.727 [1.726]	1.701(6)	1.685 [1.684]
B(4)–B(8)	1.766(16)	1.783 [1.780]	1.770(5)	1.763 [1.761]	{1.759}	1.758 [1.755]	1.837(6)	1.810 [1.835]
B(2)–B(10)	1.775(16)	1.779 [1.780]	1.775(5)	1.778 [1.780]	{1.747}	1.745 [1.745]	1.850(6)	1.825 [1.821]
B(1)–B(3)	1.658(17)	1.694 [1.689]	1.707(5)	1.705 [1.698]	{1.712}	1.712 [1.712]	1.689(6)	1.688 [1.678]

^a In the results of all the calculations it is noted that all the distances from iridium to boron are somewhat longer than those observed experimentally. We have found this to be a general feature in DFT calculations of the structure of metallaboranes of second and third-row transition elements, using the same basis-sets as those used here, for which we have reported on ruthenaboranes [61] and platinumaboranes [62]. Other calculated intercluster connectivities, e.g., interboron distances, much more closely match those determined experimentally.

position is on the open face [26]; it is most common in completely closed metallaborane cluster species, particularly those with high metal-atom content [27–29], but these also are rare. Because of this novelty, and because we calculated for the PMe_3 species **2a** rather than for the experimentally established PPh_3 species **2**, and also in order to confirm correlation of structure with measured NMR properties, boron nuclear magnetic shieldings within **2a** were calculated by the DFT-GIAO method (Table 2; see also Fig. 4 below). These DFT-GIAO//B3LYP/6-31G*/LANL2DZ results for **2a** showed an agreement with those found experimentally for **2** that was, in view of the methyl-for-phenyl approximations, and also in view of the presence of the third-row transition-element iridium, reasonable and encouraging. Thus, the deviations between the boron nuclear shieldings calculated for **2a** and those measured experimentally for **2** were all within ca. 8 ppm. In particular both measured and calculated values concurred in being diagnostically different to those for non-bridged **5** of *isonido* type B. The principal deviations between experimental and calculated shielding values for **2** versus **2a** were for the {B(8),B(10)} and {B(2),B(4)} positions directly bound to the iridium atom, and for the B(5) and B(6) positions flanking the B(4)B(8) and B(2)B(10) pairs. These variations between phenyl experimental **2** and methyl calculated **2a** were similar to the variations between methyl calculated **2a** and those calculated for the PH_3 analogue [7,7,7-(PH_3)₂H- μ -3,7-H-*isonido*-7-IrB₉H₈-9-(PH_3)] **2b**, also included in Tables 1 and 2 for comparison. These results demonstrate that the experimental matching of NMR to structure was reasonable and self-consistent, again indicating that the use of the P-methyl variant **2a** as a model for P-phenyl **2** was satisfactory, and also confirming the general structure of the compound. As mentioned, both measured and calculated boron magnetic shieldings were quite different from those found experimentally for compound **5**. Additionally, ambiguities arising from the use of HYDEX-type programmes [30,31] for the location of crys-

tallographically unlocatable hydrogen atoms are cleared by the DFT work; in the original work [24,25] all four possible locations implied by schematics **XIII** and **XV** were not sufficiently differentiated from each other in the HYDEX work. The DFT calculations allied with the ¹¹B shieldings now confirm **XV**.

As part of this work we also describe a previously unreported 10-vertex *isonido* {IrB₉} species, compound **10**, a Type-A variant. This was isolated as a purple crystalline material in about 3% yield from the reaction between PPh_3 and [6,6-(PPh_3)₂-6-H-*nido*-6-IrB₉H₁₃] (**14**, of conventional *nido* 10-vertex structure) in solution in refluxing 1,2-dichloromethane. Proton NMR spectroscopy on **10** (Table 3) shows resonances at $\delta(^1\text{H})$ ca. –8.5 and ca. –4.5 ppm (compare –8.7 and –4.4 ppm for compound **2** above). A crystal and molecular structure was obtained by single-crystal X-ray diffraction analysis (Fig. 2, left), making use

Table 3

Measured^a and calculated $\delta(^{11}\text{B})$ chemical shifts for compound **10** and its related P-methyl and P-hydryl models **10a** and **10b**

Vertex	Compound 10		Measured 10 ^a	
	Calculated $\delta(^{11}\text{B})$		$\delta(^{11}\text{B})$	$\{\delta(^1\text{H})\}$
	10a	[10b]		
3	+27.3	[+31.4]	+32.3	{+6.82 ^b }
8, 10	+9.0, +11.0	[+9.1, +12.6]	+7.0, +6.0	{+4.04 ^c }
1	–3.8	[–2.9]	–0.8	{+4.23}
9	–16.4	[–24.6]	–10.4 ^d	
5, 6	–20.1, –24.1	[–19.3, –21.5]	–21.7{–0.16}, –24.0{–0.10},	
2, 4	–18.6, –23.7	[–17.5, –22.1]	–25.8 (2B)	{–0.54, –2.00}
Ir–H(3,7)				{–4.04}
Ir–H(7)				{–8.60 ^e }

^a This work; CDCl_3 at 294–300 K; additionally $\delta(^{31}\text{P})$ +25.6 (sharp), +17 (broad) and +11.5 (sharp).

^b Strong coupling to $\mu\text{H}(3,7)$ exhibited in the [¹H–¹H]-COSY spectrum and in ¹H–{¹¹B(selective)} experiments.

^c Site of *ortho*-phenylene substituent.

^d Doublet ²J(³¹P–¹¹B) ca. 145 Hz.

^e Unresolved overlapping doublet of doublets of doublets, with all three ³J(³¹P–¹H) in region ca. 10–25 Hz.

Table 2

Chemical shifts $\delta(^{11}\text{B})$ as measured^a for Compounds **2** and **5** and as calculated for the P-methyl models **2a** and **5a** and for the P-hydryl models (see text) **2b**, **12b** and **12c**^b

Vertex	Compound 2 ^c			Compound 5		Models 12c , 12a and 12b		
	Measured 2	Calculated (mean) for:		Measured for 5	Calculated for 5a	Calculated for:		
		P-methyl 2a	[P-hydryl 2b]			[P-methyl 12c]	P-methyl 12a	[P-hydryl 12b]
3	+25.4	+22.7	[+26.5]	+59.7	{+68.7}	{+58.1}	+67.4	[+71.9]
8, 10	–7.0	+1.1, +2.5 (+1.8)	[–4.6]	+29.0, +23.6	{+38.3, +26.0}	{+27.9}	+33.5, +20.1	[+31.8, +32.9]
1	–8.2	–6.0	[–4.7]	+9.5	{+6.5}	{+10.6}	+10.8	[+11.0]
9	–11.1	–12.7	[–11.2]	–5.6	{–12.8}	{–5.1}	–10.4	[–17.3]
5, 6	–32.3	–26.2, –25.0 (–25.6)	[–25.5]	–8.2, –16.9	{–6.8, –17.7}	{–16.2}	–7.6, –5.2	[–6.9, –11.6]
2, 4	–30.0	–25.6, –22.8 (–24.2)	[–23.5]	–19.1, –26.8	{–13.3, –24.9}	{–17.2, –21.6}	–24.0, –12.2	[–12.8, –22.2]

^a Measured data taken from Ref. [24]; CD_2Cl_2 , 294–300 K.

^b **12a** is the non-chlorinated analogue of **5a**, viz. [7-(PMe_3)₂- μ -7^P,10^C-($\text{Me}_2\text{P-ortho-C}_6\text{H}_4$)-*isonido*-7-IrB₉H₇-9-(PMe_3)]]; **12b** is the P-hydryl equivalent[7-(PH_3)₂- μ -7^P,10^C-($\text{H}_2\text{P-ortho-C}_6\text{H}_4$)-*isonido*-7-IrB₉H₇-9-(PH_3)]], and **12c** is the non-*ortho*-cycloboronated non-chlorinated ‘parent’ P-methyl species [7,7-(PMe_3)₂-*isonido*-7-IrB₉H₈-9-(PMe_3)].

^c For compound **2** the calculated values from **2a** do not quite display mirror-symmetry; for **2**, the rocking between the enantiomers across the {Ir(7)B(9)B(1)B(3)} pseudo-mirror plane will have a very low activation energy, resulting in the observations of mean shieldings within each the ¹¹B(8,10), ¹¹B(5,6) and ¹¹B(2,4) pairs.

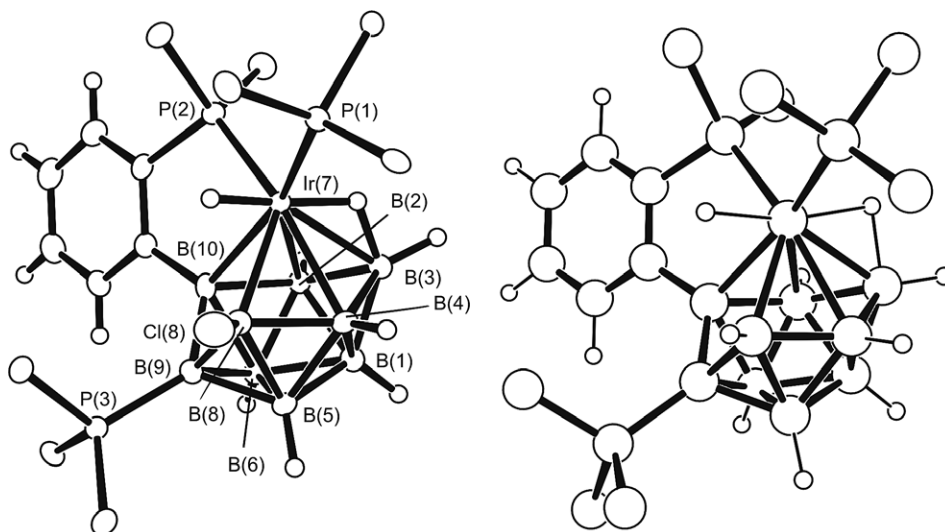


Fig. 2. ORTEP-3 drawings [60] of (left-hand diagram) the crystallographically determined molecular structure of $[7-(\text{PPh}_3)\text{-}\mu\text{-}7^{\text{P}}, 10^{\text{C}}\text{-(Ph}_2\text{P-ortho-C}_6\text{H}_4\text{)-}7\text{-H-}\mu\text{-}3, 7\text{-H-isonido-}7\text{-IrB}_9\text{H}_8\text{-}9\text{-(PPh}_3\text{)}]$ (**10**), and (right-hand diagram) the DFT-calculated molecular structure of $[7-(\text{PMe}_3)\text{-}\mu\text{-}7^{\text{P}}, 10^{\text{C}}\text{-(Me}_2\text{P-ortho-C}_6\text{H}_4\text{)-}7\text{-H-}\mu\text{-}3, 7\text{-H-isonido-}7\text{-IrB}_9\text{H}_8\text{-}9\text{-(PMe}_3\text{)}]$ (**10a**), used to model compound **10** in DFT calculations. In the crystallographically determined structure, the B(8) vertex holds a hydrogen atom (with 90% occupancy, compound **10** proper) or a chlorine atom (with a 10% partial occupancy, as illustrated, compound **11**, see text). For clarity methyl hydrogen atoms are omitted. Selected interatomic dimensions are given in Table 1.

of a crystallographic data set obtained using synchrotron-generated X-radiation. All heavy atoms were located and, additionally, centres of electron density corresponding to (a) an IrH *endo*-terminal hydrogen atom and (b) an IrHB bridging hydrogen atom to the B(3) position were apparent in the difference map; these both refined in reasonable positions. These locations concurred with those found by an XHYDEX calculation [30,31], as well as by DFT calculations (see following paragraph). Compound **10** was then shown to be $[7-(\text{PPh}_3)\text{-}\mu\text{-}7^{\text{P}}, 10^{\text{C}}\text{-(Ph}_2\text{P-ortho-C}_6\text{H}_4\text{)-}7\text{-H-}\mu\text{-}3, 7\text{-H-isonido-}7\text{-IrB}_9\text{H}_7\text{-}9\text{-(PPh}_3\text{)}]$. The incidence of a ca. 10% partial occupancy of chlorine bound *exo* to the B(8) position instead of hydrogen also emerged from the crystallographic analysis. This corresponds to a 10% presence in the crystal of **10** of its isostructural B-chlorinated derivative $[8\text{-Cl-}7\text{-(PPh}_3\text{)-}\mu\text{-}7^{\text{P}}, 10^{\text{C}}\text{-(Ph}_2\text{P-ortho-C}_6\text{H}_4\text{)-}7\text{-H-}\mu\text{-}3, 7\text{-H-isonido-}7\text{-IrB}_9\text{H}_6\text{-}9\text{-(PPh}_3\text{)}]$ (**11**). This last compound is in fact the species in Fig. 3 of Ref. [24], for which hydrogen atoms could not be located, and which was at the time believed to represent the structure of the Type-B compound $[8\text{-Cl-}7\text{-(PPh}_3\text{)-}\mu\text{-}7^{\text{P}}, 10^{\text{C}}\text{-(Ph}_2\text{P-ortho-C}_6\text{H}_4\text{)-isonido-}7\text{-IrB}_9\text{H}_6\text{-}9\text{-(PPh}_3\text{)}]$ (**5**).

$[(\text{PPh}_3)(\text{Ph}_2\text{PC}_6\text{H}_4)\text{H}]\text{IrB}_9\text{H}_7(\text{PPh}_3)$ (compound **10**) was modelled by DFT calculation, again using methyl groups instead of phenyl on the phosphine ligands for speed of calculation, although the rigid *ortho*-cycloboronated $\{\text{C}_6\text{H}_4\}$ feature was retained as this may more substantially affect cluster structure and boron nuclear shielding, particularly at and around the B(10) site to which it is bound. For this model species, viz. $[7-(\text{PMe}_3)\text{-}\mu\text{-}7^{\text{P}}, 10^{\text{C}}\text{-(Me}_2\text{P-ortho-C}_6\text{H}_4\text{)-}7\text{-H-}\mu\text{-}3, 7\text{-H-isonido-}7\text{-IrB}_9\text{H}_7\text{-}9\text{-(PMe}_3\text{)}]$ (compound **10a**), the experimentally observed quadrilateral open face in the central 10-vertex cluster of **10** (Fig. 2, left; see also schematic cluster **XIII** above) was thence reproduced in the

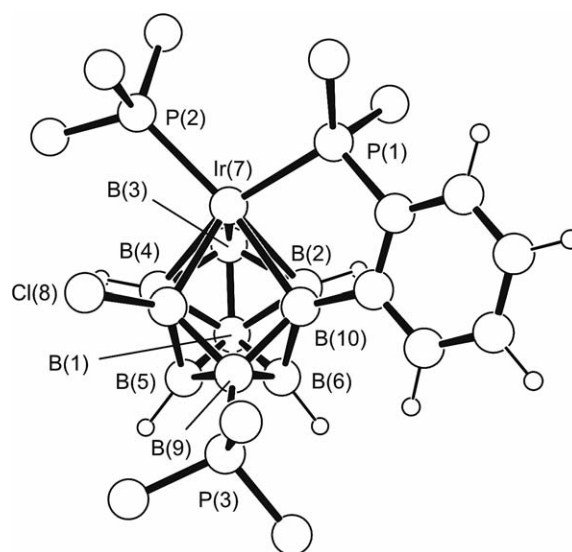


Fig. 3. ORTEP-3 drawing [60] of the DFT-calculated molecular structure of $[8\text{-Cl-}7\text{-(PMe}_3\text{)-}\mu\text{-}7^{\text{P}}, 10^{\text{C}}\text{-(Me}_2\text{P-ortho-C}_6\text{H}_4\text{)-isonido-}7\text{-IrB}_9\text{H}_6\text{-}9\text{-(PMe}_3\text{)}]$ (**5a**), used to model $[8\text{-Cl-}7\text{-(PPh}_3\text{)-}\mu\text{-}7^{\text{P}}, 10^{\text{C}}\text{-(Ph}_2\text{P-ortho-C}_6\text{H}_4\text{)-isonido-}7\text{-IrB}_9\text{H}_6\text{-}9\text{-(PPh}_3\text{)}]$ (**5**) in the DFT calculations of structure and nuclear shielding. For clarity methyl hydrogen atoms are omitted. Selected interatomic dimensions are given in Table 1.

energetically minimised structure (Fig. 2, right), and the general non-organyl dimensions calculated for **10a** were all generally similar to those found experimentally for **10** (Table 1). This correspondence indicates that the use of **10a** as a model for **10** was satisfactory. This was further confirmed by the results of DFT-GIAO boron magnetic nuclear shielding calculations on the minimised structure for **10a**, which, as with **2a** above, gave a reasonable match with the values observed experimentally for **10** (Table 3). This agreement showed that the experimental matching of NMR to

structure was in fact self-consistent, and gave additional confirmation of the general structure of compound **10** as in Fig. 2, as well as further confirmation of the applicability of the linked calculational/experimental approach.

There is a close match of the experimental and calculated geometries of these Type-A species **2**, **2a**, **10** and **10a** with the geometry reported experimentally for the Type-B compound [8-Cl-7-(PPh₃)-μ-7^P,10^C-(Ph₂P-*ortho*-C₆H₄)-*isonido*-7-IrB₉H₆-9-(PPh₃)] (**5**) in our original work [24], for which hydrogen atoms were not locatable. These close similarities suggest that the structure reported for **5** in our early work is in fact that of the Type-A compound [8-Cl-7-(PPh₃)-μ-7^P,10^C-(Ph₂P-*ortho*-C₆H₄)-7-H-μ-3,7-H-*isonido*-7-IrB₉H₇-9-(PPh₃)] (**11**), i.e., with the same formulation and substituent positioning as **5**, but now with the two extra hydrogen atoms that distinguish Type A from Type B. This supposition is substantiated in the following paragraphs. An implication is that compound **11** readily forms from **5** by reaction with solvent upon attempted recrystallisation. In our experimentation for the present work we have also observed a specific such Type-B-to-Type-A ready conversion, although we have not been able to substantiate the precise nature of the individual species involved (components **G_B** and **G_C**, see experimental section below, of Type-B and Type-A characteristics respectively). In any event, it is of obvious interest to calculate both structure and boron nuclear shielding for Type-B species such as **5**, in order to see whether the calculated shieldings match those observed experimentally, and thence to reasonably presume that a calculated structure that gives the matching nuclear shieldings is a good model for the true molecular structure.

Initial calculations involved the P-methyl non-*ortho*-cycloboronated non-chlorinated ‘parent’ model [(PMe₃)₂-IrB₉H₈(PMe₃)] **12c**, which minimised energetically to give an unbridged *isonido*-type geometry **XIV** (for dimensions see Table 1) and which then gave a boron nuclear shielding pattern that mimicked that found experimentally for **5** and its analogues [24]; in particular the very low nuclear shielding of B(3) was reproduced. Thence, by steps, the two *ortho*-cycloboronated species **12b** (P-hydryl) and **12a** (P-methyl) were calculated, and finally the 8-chloro *ortho*-cycloboronated P-methyl species **5a** (Fig. 3), the direct P-methyl analogue of the experimentally isolated P-phenyl species **5**. As with the type-A compound **2** above, the calculated boron nuclear shieldings for **5a** paralleled those determined experimentally for **5**, with similar deviations as for **2a** between experimental and calculated values (Table 2; see also Fig. 4 below).

Selected interatomic distances for the Type-B compounds **5a**, **12a**, **12b** and **12c** are given in Table 1 above. It seems apparent from these calculated dimensions that the Type-B structure is further along the *closo*–*isonido*–*isocloso* continuum towards *isocloso* than are the compounds of Type A, with Ir(7)–B(9) for Type B being shorter by between 0.1 and 0.2 Å, and B(8)–B(10) for Type B longer by between 0.1 and 0.3 Å. There are also other dif-

ferences, with B(5)–B(9) and B(6)–B(9) longer in Type B than in Type A, whereas the B(4)–B(8) and B(4)–B(10) distances are shorter. Of particular significance is the Ir(7)–B(3) distance, shorter in Type B, where it is unbridged, than in Type A, where it has a hydrogen bridge. Compared to Type A species, the iridium atom is held somewhat more intimately by the *pentahapto* boron framework in Type-B species, as discussed below.

These general and specific conclusions about structure are supported by the calculated NMR shieldings (Table 2

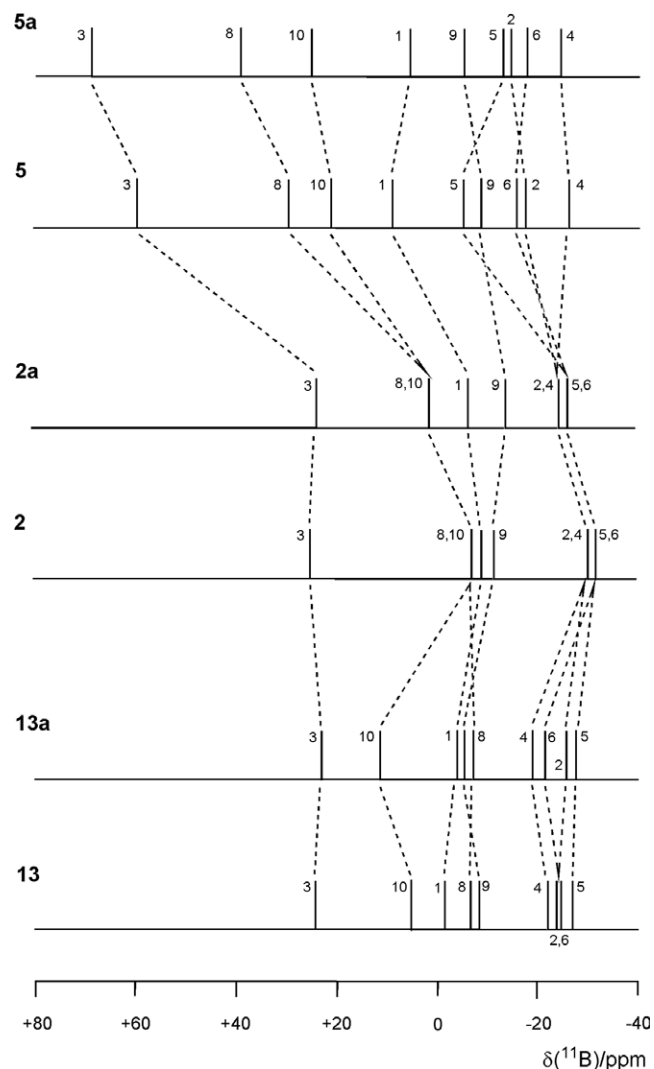


Fig. 4. Stick diagrams representing the measured and calculated ¹¹B nuclear shieldings in 10-vertex {IrB₉} metallaboranes, expressed as NMR chemical shifts δ(¹¹B): as calculated and measured for the *isonido* Type-B species **5** and **5a** (top two traces); as calculated and measured for the *isonido* Type-A species **2a** and **2** (centre two traces), and as calculated and measured for the classically *closo*-structured **13a** and **13** (bottom two traces). There are close similarities between the shieldings for classical *closo* and for *isonido* Type A, suggesting similar electronic structures: Type A can thus perhaps be regarded as ‘stretched’ *closo*. Type B, on the other hand, is more significantly different, suggesting a bigger perturbation of the overall electronic structure from that of classical *closo*, although that the principal changes are associated with just three sites adjacent to the metal centre, and that there is a similar ordering of relative shieldings, suggest a relatively localised perturbation.

and Fig. 4), which mimic those observed experimentally. In particular, the diagnostically low Type-B shielding of the B(3) nucleus, which contrasts to the higher shielding of this position in Type-A species, is reasonably reproduced. Additionally, Type A and Type B are clearly differentiated by their overall boron nuclear shielding patterns. In terms of $\delta(^{11}\text{B})$ values, type A has B(3) to low field (ca. +20 to +30 ppm), B(1), B(8), B(9) and B(10) at lower intermediate field (ca. +10 ppm) and B(2), B(4), B(5) and B(6) at higher field (ca. –30 ppm); whereas type B has B(8) and B(10) to low field (ca. +30 ppm) and B(3) at very low field (ca. +60 to +70 ppm), with only B(9) at lower intermediate field (ca. +10 ppm) and with B(9), B(2), B(4), B(5) and B(6) all at intermediate to high field (ca. +5 to ca. –30 ppm). These similarities and differences can be clearly be seen by consideration of Fig. 4.

To substantiate further that the overall techniques are viable for these third-row transition-element $\{\text{MB}_9\}$ species, we also report here the results of an all-atom single-crystal X-ray diffraction analysis for $[7\text{-(PPh}_3\text{)}-\mu\text{-}7^{\text{P}}, 8^{\text{C}}\text{-(Ph}_2\text{P-ortho-C}_6\text{H}_4\text{)}\text{-}7\text{-H-closo-}7\text{-IrB}_9\text{H}_6\text{-}3,9\text{-(PPh}_3\text{)}_2]$ (**13**) (Fig. 5), together with its measured ^1H and ^{11}B NMR properties (Table 4). Compound **13** has also been isolated as part of this work and has unambiguous classical *closo* structure (Fig. 5 and Table 1; see also schematic cluster structure X above). It is also robust in solution, and so there is not any doubt that the experimentally determined NMR parameters (Table 4) correspond to the molecular structure (Fig. 5). We thence carried out DFT calculations of structure and of nuclear shielding on its methyl-for-phenyl-substituted model $[7\text{-(PMe}_3\text{)}-\mu\text{-}7^{\text{P}}, 8^{\text{C}}\text{-(Me}_2\text{P-ortho-C}_6\text{H}_4\text{)}\text{-}7\text{-H-closo-}7\text{-IrB}_9\text{H}_6\text{-}3,9\text{-(PMe}_3\text{)}_2]$ (**13a**). For both cluster structure and shielding, the calculated values for **13a** match with those observed by experiment for **13** (Fig. 5 and Tables 1 and 4), supporting the soundness of the approach to compounds of this nature, and in particular giving confidence to the conclusions about the constitutions and different natures of the two types, A

Table 4

Measured^a and calculated chemical shift data for compound **13** and its related P-methyl model **13a** and P-hydryl model **13b**

Assignment	$\delta(^{11}\text{B})$		$\delta(^{11}\text{B})$ (13) ^a	$\delta(^1\text{H})$ (13) ^a
	Calculated (13a)	[13b]		
3	+22.3	[+7.8]	+24.2 ^b	
10	+11.4	[+2.2]	+5.9	
1	–4.6	[–8.9]	–1.5	+2.87 ^c
8	–6.6	[–12.9]	–7.5	+3.05
9	–5.7	[–23.0]	–8.6	
4	–19.0	[–31.6]	–21.2	+0.1
2, 6	–25.9, –21.7	[–34.9, –29.6]	–22.1(2)	–0.35, –1.73
5	–26.9	[–36.1]	–26.2	–0.93
IrH				–4.17 ^d

^a This work; CDCl_3 , 294–300 K; additionally $\delta(^{31}\text{P})$ +30.5 (sharp), +24.2 (sharp) and +17.9 (broad, 2P, two overlapping resonances).

^b Doublet $^2J(^{31}\text{P}\text{-}^{11}\text{B})$ ca. 155 Hz.

^c Doublet, probably coupled to P(3), $^3J(^{31}\text{P}\text{-}^1\text{H})$ 14 Hz.

^d Overlapping doublet of doublet of doublets; $^nJ(^{31}\text{P}\text{-}^1\text{H})$ 22.0, 25.7 and 30.5 Hz.

and B, for the more problematical 10-vertex *isonido*-structured species. Compound **13** was isolated in yields of up to 33% from the reactions of PPh_3 with $[6,6\text{-(PPh}_3\text{)}_2\text{-}6\text{-H-nido-}6\text{-IrB}_9\text{H}_{13}]$ (**14**).

The reactions of PPh_3 with $[6,6\text{-(PPh}_3\text{)}_2\text{-}6\text{-H-nido-}6\text{-IrB}_9\text{H}_{13}]$ (**14**) also yielded its known *ortho*-cycloboronated variant $[6\text{-(PPh}_3\text{)}-\mu\text{-}6^{\text{P}}, 5^{\text{C}}\text{-(Ph}_2\text{P-ortho-C}_6\text{H}_4\text{)}\text{-}6\text{-H-nido-}6\text{-IrB}_9\text{H}_{12}]$ (**15**), in trace quantities. Compound **15** has figured much as a starting material or as a by-product in iridaborane reaction chemistry [32–34], but its crystallographic characterisation has previously proved elusive. As part of this work we have finally been able to isolate crystals suitable for a single-crystal X-ray diffraction analysis (Fig. 6). The compound is of straightforward classical *nido* 10-vertex cluster configuration analogous to that of the binary borane model *nido*- $\text{B}_{10}\text{H}_{14}$. The presence of the cyclised

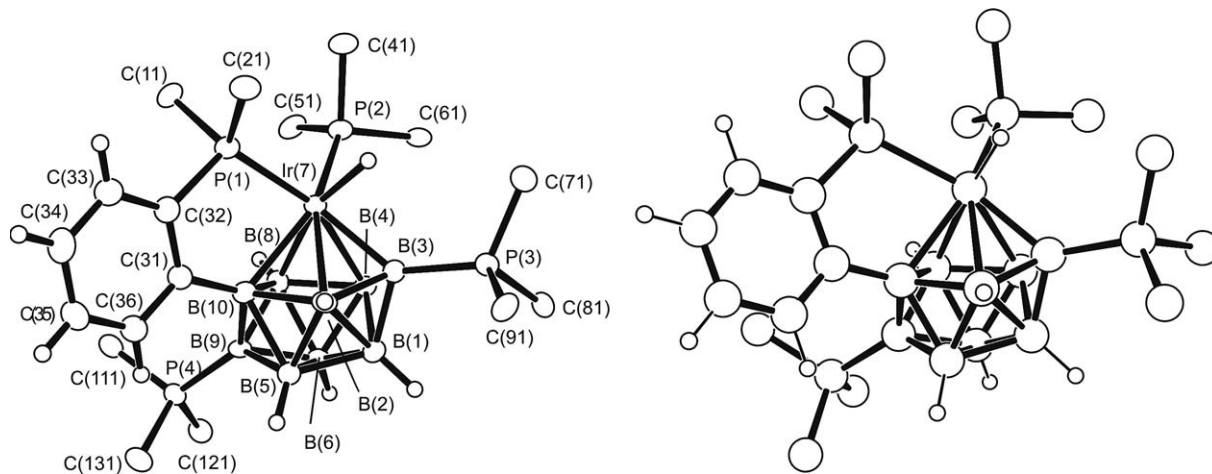


Fig. 5. ORTEP-3 drawings [60] of (left-hand diagram) the crystallographically determined molecular structure of $[7\text{-(PPh}_3\text{)}-\mu\text{-}7^{\text{P}}, 8^{\text{C}}\text{-(Ph}_2\text{P-ortho-C}_6\text{H}_4\text{)}\text{-}7\text{-H-closo-}7\text{-IrB}_9\text{H}_6\text{-}3,9\text{-(PPh}_3\text{)}_2]$ (**13**) and (right-hand diagram) the DFT-calculated molecular structure of $[7\text{-(PMe}_3\text{)}-\mu\text{-}7^{\text{P}}, 8^{\text{C}}\text{-(Me}_2\text{P-ortho-C}_6\text{H}_4\text{)}\text{-}7\text{-H-closo-}7\text{-IrB}_9\text{H}_6\text{-}3,9\text{-(PMe}_3\text{)}_2]$ (**13a**), used to model **13** in the DFT calculations. For clarity methyl hydrogen atoms are omitted. Selected interatomic dimensions are given in Table 1.

ortho-phenylene group causes a small elongation of the B(5)–B(10) *nido* 10-vertex ‘gunwale’ vector compared to that [35] in the uncyclised compound **14**: 2.052(7) in **15** versus 1.997(16) Å in **14**. The other B(7)–B(8) ‘gunwale’ vector remains essentially unchanged, with values of 2.016(7) for **15** and 1.993(16) Å for **14**.

Whatever the electronic structures of the two 10-vertex *isonido* cluster variants A and B – and it would appear that these are significantly different, judging by the differences in ^{11}B shielding properties (Fig. 4) which will be critically dependent upon electronic structure – it would appear that the formal oxidation state of iridium in the two clusters may differ by two units. Whether it is best regarded as iridium(I) in A and iridium(III) in B, or two units higher in each case, i.e. iridium(III) in Type A and iridium(V) in Type B, is an interesting question. Another possibility is iridium(I) in Type B and iridium(III) in Type A, as discussed below. Certainly there is no need to invoke other than conventional d^6 iridium(III) in compound **13** of straightforward classical *closo* constitution. The constituents of the cluster of *isonido* Type-A compound **2** make it isoelectronic with classical *closo* **13**. The cluster opening to *isonido* observed for **2** could therefore be a ‘flexibility’ distortion associated with the accommodation of two extra hydrogen atoms, with no catastrophic internal changes in electronic structure (Fig. 4). This conclusion is perhaps supported by the similarities in ^{11}B shielding patterns between straightforward *closo* (e.g., compound **13**) and *isonido* Type A (Tables 2–4) that could be taken to indicate no catastrophic differences in internal electronic structure. This would imply formal iridium(III) in Type-A compound **2**. Compared to **2**, the Type-B *isonido* cluster of compound

5 lacks two hydrogen atoms, and therefore has two electrons fewer than either the *closo*-shaped cluster of compound **13** or the *isonido*-shaped Type-A cluster of compound **2**. The larger differences in ^{11}B nuclear shieldings (Table 2 and Fig. 4) suggest more fundamental differences in electronic structure when **5** is compared to **2** and **13**. A classical cluster opening from *closo* to classical *nido* requires two extra cluster electrons. If the opening here from *closo* to *isonido* also requires two electrons, then the two electrons would formally originate from the iridium core to give it a d^4 iridium(V) configuration. This would imply a four-orbital contribution to the cluster metal centre which thence could be invoked to explain the unusual *isonido* geometry, as opposed to the classical *nido* which would have a three-orbital contribution from all cluster constituents. Conversely, however, the distortion could be a manifestation of an incipient ‘slippage’ related to that of the ‘slipped-*closo*’ seven-vertex and 13-vertex species mentioned above (schematics IV and VI). This would be visualisable in terms of essentially square-planar d^8 iridium(I) character with a tendency towards a formal two-orbital involvement with the cluster, rather than the conventional three-orbital involvement. However, the iridium-to-boron distances when **2** and **5** are compared suggest a more intimate involvement of the iridium centre with the borane residue in the Type-B compound **5**, rather than a less intimate ‘slipped’ configuration: all the iridium-to-boron distances in **5** are in fact either essentially the same or shorter than those in compound **2**.

3. Conclusions

Although the electronic origins of the 10-vertex *isonido* $\{\text{MB}_9\}$ structures, and variations among these structures, remain unresolved, the work reported here now more confidently defines the general structural type and the NMR properties associated with the type. Within the basic 10-vertex *isonido* skeletal geometry, two variants are substantiated. Variant A has a metal-to-boron hydrogen bridge that is not associated with an open-face boron atom. This characteristic is very unusual in known metallaborane chemistry. Variant A also has an *endo*-terminal iridium-hydride unit (schematic XV above). Type B, by contrast, does not have these two hydrogen characteristics (schematic XIV above). Variant A is now well characterised crystallographically. Type B *isonido* remains crystallographically uncharacterised within the $\{\text{IrB}_9\}$ system, but DFT calculations show the structural characteristics that are to be anticipated. As far as we are aware, the only crystallographically characterised Type B species remains the $\{\text{MCB}_8\}$ metallacarbaborane [3-(OMe)-7-(PPh₃)- μ -7^P, 10^C-(Ph₂P-*ortho*-C₆H₄)-*isonido*-7,8-IrCB₈H₆-10-(OH)], reported a quarter of a century ago [36]. The work presented here highlights the usefulness, in the elucidation of metallaborane systems, of the synergic alliance of (a) crystallography (including HYDEX and XHYDEX [30,31] for the location of crystallographically unlocated hydrogen atoms), (b) multinuclear NMR spectroscopy and

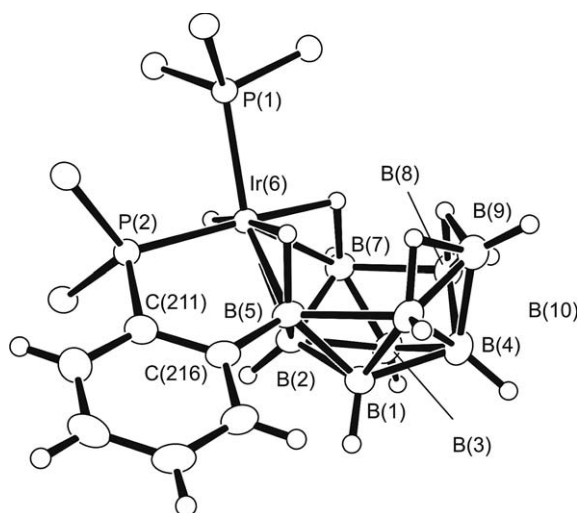


Fig. 6. ORTEP-3 drawing [60] of the crystallographically determined molecular structure of [6-(PPh₃)- μ -6^P, 5^C-(Ph₂P-*ortho*-C₆H₄)-6-H-*nido*-6-IrB₉H₁₂] (**15**). Selected interatomic distances (in Å) are as follows: from Ir(6) to P(1) 2.3186(10), P(2) 2.2941(12), H(Ir) 1.68, B(2) 2.249(4), B(5) 2.236(4), B(7) 2.297(4), H(5,6) 1.76(6) and H(6,7) 1.79(5); B(5)–C(216) is 1.588 (5) B(5)B(10) is 2.052(7) and B(7)–B(8) is 2.016(7). Selected angles (in deg.) are P(1)–Ir(6)–P(2) 97.46(4), P(2)–C(211)–C(216) 115.3(3), C(216)–B(5)–Ir(6) 116.7(3), B(5)–Ir(6)–P(2) 81.32(12) and C(216)–B(5)–Ir(6) 116.7(3).

(c) DFT calculations for structure and nuclear shielding. In this regard, the successful application of this linked approach to metallaboranes of the third-row transition element iridium is particularly encouraging, since many of the most interesting metallaborane systems involve late third-row transition elements.

4. Experimental

4.1. General

Dried and degassed solvents were used throughout. Reactions were carried out under dry dinitrogen, although subsequent compound isolation using preparative chromatography was carried out in air. [6,6-(PPh₃)₂-6-*nido*-6-IrB₉H₁₃] (**14**) was prepared as described previously [32–34]. Thin-layer chromatography (TLC) was carried out using 1 mm layers of silica-gel G (Fluka, type GF254) made from water slurries on glass plates of dimensions 20 × 20 cm followed by drying in air at 80 °C. HPLC was performed on a 21 mm × 25 cm column (Knauer, Lichosorb Si60, 7 mm) with detection by change in the UV absorption of the eluted liquid at $\lambda = 254$ nm. NMR spectroscopy was performed at ca. 5.9 T, 9.4 T and 11.4 T (fields corresponding to 250, 400 and 500 MHz ¹H frequencies respectively) using commercially available instrumentation and established techniques [37–39], with overall procedures as adequately described and enunciated elsewhere [40–43]. Chemical shifts δ are given in ppm relative to $\varepsilon = 100$ MHz for $\delta(^1\text{H})$ (± 0.05 ppm) (nominally TMS), $\varepsilon = 32.083972$ MHz for $\delta(^{11}\text{B})$ (± 0.5 ppm) (nominally [F₃BOEt₂] in CDCl₃) [44] and $\varepsilon = 40.480730$ MHz for $\delta(^{31}\text{P})$ (± 0.5 ppm) (nominally 85% aqueous H₃PO₄). ε is as defined by McFarlane [45].

4.2. Isolation of [(PPh₃)(Ph₂PC₆H₄)HIrB₉H₆Cl(PPh₃)] (**10**) and [(PPh₃)(Ph₂PC₆H₄)HIrB₉H₆(PPh₃)₂] (**13**)

A solution of [6,6-(PPh₃)₂-6-*H-nido*-6-IrB₉H₁₃] (**14**; 106 mg, 128 μmol) and PPh₃ (67 mg, 260 μmol) in 1,2-dichloroethane (5 ml) was heated at reflux for 2 h under a nitrogen atmosphere. After cooling, the solvent was removed on a Schlenk line at ambient temperature, the residue dissolved in dichloromethane, filtered through a silica gel plug, reduced in volume, and applied to a number of preparative TLC plates, which were then developed using CH₂Cl₂/*n*-C₆H₁₂ (80/20) as liquid phase. Three bands were apparent; **A**, R_F 0.7, colourless (observed under UV illumination); **B**, R_F 0.4, strong yellow and **C**, R_F 0.35, yellow. A number of relatively faint blue and purple bands were also apparent, ranged below band **C** down to the baseline at R_F zero. Band **A** was identified as PPh₃. Bands **B** and **C** were re-chromatographed, affording, for component **B**, yellow [7-(PPh₃)- μ -7^P,8^C-(Ph₂P-*ortho*-C₆H₄)-7-*H-closo*-7-IrB₉H₆-3,9-(PPh₃)₂] (compound **13**) (63 mg, 42 μmol , 33%) and, for component **C**, 6 mg of a yellow material. NMR spectroscopy clearly indicated that component **C** was an analogue

of compound **5**. Measured NMR data for component **C** (CDCl₃, 294–297 K) are as follows: $\delta(^{11}\text{B})$ +23.0 (1B; doublet, ² $J(^{31}\text{P}-^{11}\text{B})$ ca. 155 Hz), –5.2 (2B) singlet, –7.5 (2B), –25.2 (2B) and –26.9 (2B); $\delta(^1\text{H})$ +2.60 (1H), +2.35 (1H), –0.69 (2H), –1.77 (2H) and –5.40 (1H; doublet of doublets, ² $J(^{31}\text{P}-^1\text{H})$ 50 and 25 Hz); $\delta(^{31}\text{P})$ +16.8 (sharp singlet) and ca. +17 (broad). However, attempts to obtain suitable single crystals of **C** for X-ray diffraction analysis were unsuccessful and the compound remains incompletely characterised.

In a second variant of the reaction, [6,6-(PPh₃)₂-6-*H-nido*-6-IrB₉H₁₃] (**14**, 84 mg, 107 μmol) and PPh₃ (56 mg, 210 μmol) were heated in solution in 1,2-dichloroethane (5 ml) at reflux for the shorter time of 1 h. TLC separation using 80/20 CH₂Cl₂/*n*-C₆H₁₂ as liquid phase afforded three bands: **D**, R_F 0.7 yellow; **E**, R_F 0.5–0.4 yellow; and **F**, R_F 0.4–0.1, mixed blue and purple. Band **D** was subjected to HPLC separation (40/60 CH₂Cl₂/*n*-C₆H₁₂, 10 ml min^{–1}) giving a single component (R_T 12.7 min), identified from its ¹¹B, ¹H and ³¹P NMR spectra as [6-(PPh₃)- μ -6^P,5^C-(Ph₂P-*ortho*-C₆H₄)-6-*H-nido*-6-IrB₉H₁₂] **15**. Compound **15** is previously reported [32–35], but not previously substantiated crystallographically. Single-crystals suitable of **15** for X-ray diffraction analysis were therefore obtained, by diffusion of C₆H₁₄ into a solution of the compound in CDCl₃. Band **E** was identified as compound **13** (173 mg, 11 μmol , 10%). The mixed purple and blue bands **F**, ranging from R_F ca. 0.1 to ca. 0.4, were significantly stronger in this experiment, and were subjected to HPLC separation (50/50 CH₂Cl₂/*n*-C₆H₁₂, 10 ml min^{–1}). Two strong blue-purple components, **G** (R_T 12.8 min) and **H** (R_T 14.6 min), were eluted. Repeated HPLC separation of **G** gave two components, **G_A** (blue, R_T 16.0 min) and **G_B** (blue, R_T 19.6 min). Attempts at crystallisation of the bands and characterisation were successful in the case of component **G_A**: thus, a layered *n*-C₆H₁₂/C₆H₆/CH₂Cl₂ diffusion gave blue crystals of [7-(PPh₃)- μ -7^P,10^C-(Ph₂P-*ortho*-C₆H₄)-7-*H- μ -3,7-*H-isonido*-7-IrB₉H₈-9-(PPh₃)*] (**10**) (2.7 mg, 2.2 μmol , 2%). X-ray diffraction analysis showed that the crystals had a partial (10%) crystal occupancy by [8-Cl-7-(PPh₃)- μ -7^P,10^C-(Ph₂P-*ortho*-C₆H₄)-7-*H- μ -3,7-*H-isonido*-7-IrB₉H₇-9-(PPh₃)*] (**11**), i.e., an overall formulation of [(PPh₃)(Ph₂PC₆H₄)HIrB₉H₆Cl_{0.1}(PPh₃)]. In the case of component **G_B** preliminary ¹¹B, ¹H and ³¹P NMR spectroscopy in CDCl₃ solution suggested an *isonido* iridanonaborane of type **B**, similar in constitution to Type-A compound **10**, but with no IrH terminal or IrHB bridging hydrogen atoms; it had a characteristic type-B ¹¹B(3) resonance at $\delta(^{11}\text{B})$ +64.0 ppm. However, relatively rapid reaction with the solvent occurred, giving a solution containing principally a single component **G_C** that appeared to be a variant of compound **10**, now with IrH terminal and IrHB bridging hydrogen atoms, at $\delta(^1\text{H})$ –4.05 and –8.60 ppm, respectively; also, the diagnostically very low-field ¹¹B(3) resonance had shifted to a type-A position at $\delta(^{11}\text{B})$ +32.5 ppm. Measured NMR data for component **G_B** (CDCl₃, 294–297 K) are as follows: $\delta(^{11}\text{B})$ +64.0, +29.6

(2B), +10.8, −1.9 [doublet, $^2J(^{31}\text{P}-^{11}\text{B})$ ca. 150 Hz], −7.9, −15.4, −16.0 and −25.4; $\delta(^1\text{H})$ +6.82, +5.22, +1.22, +0.87, −0.31 and −1.09; $\delta(^{31}\text{P})$ +49.7 (sharp), +35.5 (sharp) and +18 (broad). Measured NMR data for component **Gc** (CDCl_3 , 294–297 K) are as follows: $\delta(^{11}\text{B})$ +32.5, +6.8, −0.9, −10.5 [doublet, $^2J(^{31}\text{P}-^{11}\text{B})$ ca. 147 Hz], −21.7, −24.0 and −25.9; $\delta(^1\text{H})$ +4.23, +4.03, +0.11, −0.15, −0.54, −2.00, −4.05 and −8.60 (overlapping doublet of doublets of doublets structure, all $^nJ(^{31}\text{P}-^1\text{H})$ ca. 20–30 Hz).

4.3. Single-crystal X-ray diffraction analysis

Crystals from $[(\text{PPh}_3)(\text{Ph}_2\text{PC}_6\text{H}_4)\text{H}(\text{IrB}_9\text{H}_6\text{Cl}_{0.1}(\text{PPh}_3))]$ (**10**) suitable for the X-ray work were grown in a 5-mm glass tube from concentrated CH_2Cl_2 solution by liquid–liquid diffusion from an overlayer of *n*-pentane through an intermediate layer of benzene. The data collection was carried out using a Bruker SMART APEX2 CCD diffractometer with synchrotron radiation (SRS station 9.8, CCLRC Daresbury Laboratories, UK) [52–54]. The asymmetric unit contained half a molecule of benzene and a disordered molecule of pentane, which was refined isotropically over two positions. All non-hydrogen atoms were refined with anisotropic displacement parameters. Hydrogen atoms were refined isotropically in calculated positions with the exception of the terminal and the bridging metal hydrogen atoms H(7) and H(3,7). These were located in the difference map and refined freely. Their positions were confirmed using XHYDEX [30,31] which also corresponded well to those calculated using DFT. A 10% partial occupancy of the B(8)H(*exo*) site by a BCl(*exo*) unit emerged from the analysis. Crystal data are as follows. $[(\text{PPh}_3)(\text{Ph}_2\text{PC}_6\text{H}_4)\text{H}(\text{IrB}_9\text{H}_5.9\text{Cl}_{0.1}(\text{PPh}_3))\{C_6H_{12}\}_{0.5}\{C_6H_6\}]$: $C_{62}H_{67.9}B_9Cl_{0.1}IrP_3$; $M = 1199.1$, blue block, $0.05 \times 0.04 \times 0.02$ mm, triclinic, $a = 10.4823(13)$, $b = 13.2092(17)$, $c = 22.321(3)$ Å, $\alpha = 88.051(2)$, $\beta = 89.612(2)$, $\gamma = 68.215(2)^\circ$, $V = 2868.2(6)$ Å³, $D_{\text{calc}} = 1.388$ Mg m^{−3}; $\lambda = 0.6933$ Å (synchrotron, wiggler-generated, silicon-monochromated), $T = 120(2)$ K, space group $P\bar{1}$, $Z = 2$, $\mu = 2.455$ mm^{−1}, $R_1 = 0.0423$ for 14229 reflections with $I > 2\sigma(I)$, and $wR_2 = 0.0797$ for all 16997 unique reflections.

Crystals of $[(\text{PPh}_3)(\text{Ph}_2\text{PC}_6\text{H}_4)\text{H}(\text{IrB}_9\text{H}_6(\text{PPh}_3)_2)]$ (**13**) suitable for the X-ray analysis were grown in a 5-mm glass tube from a concentrated solution in CH_2Cl_2 by liquid–liquid diffusion from an overlayer of cyclohexane through an intermediate layer of toluene. The collection of data were carried out using a Bruker-Nonius KappaCCD area detector using Mo $K\alpha$ radiation generated from a Bruker-Nonius FR591 rotating-anode X-ray source. The structure was solved using standard methods [46–50]. All non-hydrogen atoms were refined with anisotropic displacement parameters. Hydrogen atoms were refined isotropically in calculated positions with the exception of the terminal metal hydride which was freely refined. XHYDEX calculation confirmed the location. The unit cell contained disordered solvent molecules that were included in the model using the PLATON/SQUEEZE procedure [51]. Crystal data are as follows.

$[(\text{PPh}_3)(\text{Ph}_2\text{PC}_6\text{H}_4)\text{H}(\text{IrB}_9\text{H}_6(\text{PPh}_3)_2)]$ (**13**): $C_{72}H_{66}B_9Ir_1P_4$; $M = 1344.7$, yellow shard, $0.20 \times 0.12 \times 0.08$ mm, monoclinic, $a = 41.1175(4)$, $b = 15.0755(2)$, $c = 29.0142(3)$ Å, $\beta = 121.541(1)^\circ$, $V = 15327.9(3)$ Å³, $\lambda = 0.71073$ Å (Mo $K\alpha$), $T = 120(2)$ K, space group $C2/c$ $Z = 8$, $\mu(\text{Mo } K\alpha) 1.862$ mm^{−1}, $R_1 = 0.0366$ for 14518 reflections with $I > 2\sigma(I)$, and $wR_2 = 0.0815$ for all 17566 unique reflections.

Crystals from $[(\text{PPh}_3)(\text{Ph}_2\text{PC}_6\text{H}_4)\text{IrB}_9\text{H}_{12}]$ (**15**) suitable for the single-crystal X-ray diffraction analysis were grown in a 5-mm o.d. glass tube from a concentrated solution in CDCl_3 , by liquid–liquid diffusion from an overlayer of *n*-hexane through an intermediate layer of benzene. The data collection was carried out using a (pre-Bruker) Nonius KappaCCD area-detector diffractometer with Mo $K\alpha$ radiation. The asymmetric unit contained half a molecule of *n*-hexane. All non-hydrogen atoms were refined with anisotropic displacement parameters. Hydrogen atoms were refined isotropically in calculated positions with the exception of the terminal and the bridging metal hydrogen atoms H(6) and H(5,6). These were located using XHYDEX [30,31]. The bridging hydrogen atom H(5,6) thence refined satisfactorily, mirroring H(6,7) which was located in the difference map. Atom H(6) was refined in a fixed position. Crystal data are as follows.

$[(\text{PPh}_3)(\text{Ph}_2\text{PC}_6\text{H}_4)\text{IrB}_9\text{H}_{12}]\{C_6H_{14}\}_{0.5}$: $C_{39}H_{49}B_9Ir_1P_2$; $M = 869.2$, yellow block, $0.43 \times 0.24 \times 0.10$ mm, triclinic, $a = 11.108(2)$, $b = 12.545(3)$, $c = 15.410(3)$ Å, $\alpha = 93.87(3)$, $\beta = 107.67(3)$, $\gamma = 104.82(3)^\circ$, $V = 1953.3(7)$ Å³, $D_{\text{calc}} = 1.478$ Mg m^{−3}; $\lambda = 0.71073$ Å (Mo $K\alpha$), $T = 150(2)$ K, space group $P\bar{1}$, $Z = 2$, $\mu = 3.528$ mm^{−1}, $R_1 = 0.0401$ for 8510 reflections with $I > 2\sigma(I)$, and $wR_2 = 0.1105$ for all 8905 unique reflections.

4.4. Computational method

Calculations carried out in this study were performed using the GAUSSIAN98 and GAUSSIAN03 packages [55–59]. Structures were initially optimised with the STO-3G* basis-sets for B, C, P, Cl, H and with the LANL2DZ basis-set for the Ir atom, using standard ab initio methods. The final optimisations, including frequency analyses to confirm the true minima, together with GIAO NMR nuclear-shielding predictions, were performed using B3LYP methodology, again with the 6-31G* basis-sets for H, B, C, P and Cl, and the LANL2DZ basis-set for the iridium atom. The GIAO NMR nuclear-shielding predictions were performed on the final optimised geometries. In each case the compounds were modelled initially using hydrogen atoms rather than phenyl groups on the phosphine ligands, and then, based on the geometries so obtained, the structural and boron nuclear shielding calculations were extended to the final P-methyl models **2a**, **5a**, **10a** and **13a**. For species **2**, **10** and **13**, the frequency analyses were carried out on the simpler PH_3 variants **2b**, **10b**, and **13b**: time constraints precluded frequency calculations on the methyl variants **2a**, **10a** and **13a**. For the experimentally less well established species **5**, however,

frequency analyses were carried out on the P-methyl model **5a**. The reasonable match of both structures and individual ^{11}B nuclear shieldings within each of the groupings {**2,2a,2b**}, {**5,5a**}, {**10,10a,10b**} and {**13,13a,13b**} supports the validity of this approach. In the results of all the structural calculations it is noted that all the distances from iridium to boron are somewhat longer than those observed experimentally. We have found this to be a general feature in DFT calculations of the structure of metallaboranes of second-row and third-row transition elements using the same basis-sets, for which we have reported on ruthenaboranes [61] and platinaboranes [62]. Other calculated intercluster connectivities, e.g., interboron distances, much more closely match those determined experimentally.

Acknowledgements

A proportion of the work has been personally financed by JB, who thanks the School of Chemistry of the University of Leeds for facilities and Professors P.J. Kocienski and M.J. Pilling for their good offices. JB and JDK thank Colin Kilner for help with crystallographic data collection and Simon Barrett for help with NMR spectroscopy. Instrumentation grants from the EPSRC are acknowledged (J/56929, K/05818, L/49505, M/83360, R/61949). We also thank CCLRC for the award of synchrotron beam time at the UK SRS Daresbury laboratory, and the EPSRC UK National X-ray Service for the collection of a crystallographic data set.

Appendix A. Supplementary data

Supplementary data associated with this article can be found, in the online version, at [doi:10.1016/j.ica.2006.01.038](https://doi.org/10.1016/j.ica.2006.01.038). Crystallographic data for the structural analysis are deposited with the Cambridge Crystallographic Data Centre, CCDC deposition nos. 290672 for **10**, 29067 for **3** and 290674 for **15**.

References

- [1] D.M.P. Mingos, *Nature (Phys. Sci.)* 236 (1972) 99.
- [2] D.M.P. Mingos, *Pure Appl. Chem.* 63 (1991) 807.
- [3] R.E. Williams, *Inorg. Chem.* 1 (1971) 210.
- [4] R.E. Williams, *Adv. Inorg. Chem. Radiochem.* 18 (1976) 67.
- [5] K. Wade, *J. Chem. Soc., Chem. Commun.* (1971) 792.
- [6] K. Wade, *Adv. Inorg. Chem. Radiochem.* 18 (1976) 1.
- [7] R.W. Rudolph, W.P. Pretzer, *Inorg. Chem.* 11 (1972) 1974.
- [8] R.W. Rudolph, *Acc. Chem. Res.* 9 (1976) 446.
- [9] R.M. Wing, *J. Am. Chem. Soc.* 89 (1967) 5599.
- [10] M.F. Hawthorne, D.C. Young, T.D. Andrews, D.V. Howe, R.L. Pilling, A.D. Pitts, M. Reintjes, L.F. Warren Jr., P.A. Wegner, *J. Am. Chem. Soc.* 90 (1968) 879.
- [11] See, for example, together with references therein: G.B. Dunks, M.F. Hawthorne, *closo*-Heteroboranes exclusive of carboranes, in: E.L. Muetterties (Ed.), *Boron Hydride Chemistry*, Academic, New York, San Francisco, and London, 1975, p. 383 (Chapter 11).
- [12] L.F. Warren Jr., M.F. Hawthorne, *J. Am. Chem. Soc.* 90 (1968) 4823.
- [13] R.M. Wing, *J. Am. Chem. Soc.* 90 (1968) 4828.
- [14] N.W. Alcock, J.G. Taylor, M.G.H. Wallbridge, *J. Chem. Soc., Dalton Trans.* (1987) 1805.
- [15] See, together with references therein: H.M. Colquhoun, T.J. Greenhough, M.G.H. Wallbridge, *J. Chem. Soc., Dalton Trans.* (1985) 761.
- [16] D.M.P. Mingos, M.I. Forsyth, A.J. Welch, *J. Chem. Soc., Chem. Commun.* (1977) 605.
- [17] D.M.P. Mingos, M.I. Forsyth, A.J. Welch, *J. Chem. Soc., Dalton Trans.* (1978) 1363.
- [18] See, for example: G.K. Barker, M. Green, T.P. Onak, F.G.A. Stone, C.B. Ungermann, A.J. Welch, *J. Chem. Soc., Chem. Commun.* (1978) 169.
- [19] See, for example, together with references therein: J.D. Kennedy, *Main Group Metal Chem.* 12 (1989) 149.
- [20] J.D. Kennedy, in: *Disobedient skeletons*, in: J. Casanova (Ed.), *The Borane–Carborane–Carbocation Continuum*, Wiley, New York, 1998, p. 85 (Chapter 3).
- [21] M.E. O'Neill, K. Wade, *Polyhedron* 2 (1983) 963.
- [22] See, for example, together with references therein: B. Štíbr, J.D. Kennedy, M. Thornton-Pett, E. Drdáková, T. Jelínek, J. Plešek, *Collect. Czech. Chem. Commun.* 57 (1992) 1439.
- [23] B. Štíbr, J.D. Kennedy, E. Drdáková, M. Thornton-Pett, *J. Chem. Soc., Dalton Trans.* (1994) 229.
- [24] J. Bould, J.D. Kennedy, M. Thornton-Pett, *J. Chem. Soc., Dalton Trans.* (1992) 563.
- [25] M. Thornton-Pett, personal communication.
- [26] See, for example, together with references therein: M.J. Carr, S.D. Perera, T. Jelínek, C.A. Kilner, B. Štíbr, J.D. Kennedy, *J. Organomet. Chem. (EUROBORON 3 Special Edition)* 690 (2005) 2857.
- [27] J.D. Kennedy, *Prog. Inorg. Chem.* 32 (1984) 519.
- [28] J.D. Kennedy, *Prog. Inorg. Chem.* 34 (1986) 211.
- [29] L. Barton, D.K. Srivastava, in: *Metallaboranes*, in: G. Wilkinson, F.G.A. Stone, E. Abel (Eds.), *Comprehensive Organometallic Chemistry II*, vol. 1, Pergamon, Elmsford, New York, 1995, p. 275 (Chapter 8).
- [30] XHYDEX, A.G. Orpen, *J. Chem. Soc., Dalton Trans.* (1980) 2509.
- [31] As implemented in G.X. Win, L.J. Farrugia, *J. Appl. Crystallogr.* 32 (1999) 837.
- [32] J. Bould, J.E. Crook, N.N. Greenwood, J.D. Kennedy, M. Thornton-Pett, *J. Chem. Soc., Dalton Trans.* (1990) 1441.
- [33] J. Bould, N.N. Greenwood, J.D. Kennedy, *J. Chem. Soc., Dalton Trans.* (1990) 1451.
- [34] J. Bould, M. Bown, R.J. Coldicott, E.J. Ditzel, N.N. Greenwood, I. Macpherson, P. MacKinnon, M. Thornton-Pett, J.D. Kennedy, *J. Organomet. Chem. (EUROBORON 3 Special Edition)* 690 (2005) 2701.
- [35] S.K. Boocock, J. Bould, N.N. Greenwood, J.D. Kennedy, W.S. McDonald, *J. Chem. Soc., Dalton Trans.* (1982) 713.
- [36] J.E. Crook, N.N. Greenwood, J.D. Kennedy, W.S. McDonald, *J. Chem. Soc., Chem. Commun.* (1981) 933.
- [37] See, for example, together with references therein: J. Schraml, J.M. Bellama, *Two-Dimensional NMR Spectroscopy*, Wiley, New York, 1982.
- [38] W.C. Hutton, T.L. Venable, R.N. Grimes, *J. Am. Chem. Soc.* 106 (1984) 29.
- [39] X.L.R. Fontaine, J.D. Kennedy, *J. Chem. Soc., Dalton Trans.* (1987) 1573.
- [40] See, for example: J. Plešek, B. Štíbr, X.L.R. Fontaine, J.D. Kennedy, S. Heřmánek, T. Jelínek, *Collect. Czech. Chem. Commun.* 56 (1991) 1618.
- [41] G. Ferguson, J.D. Kennedy, X.L.R. Fontaine, Faridoun, T.R. Spalding, *J. Chem. Soc., Dalton Trans.* (1988) 2555.
- [42] M.A. Beckett, M. Bown, X.L.R. Fontaine, N.N. Greenwood, J.D. Kennedy, M. Thornton-Pett, *J. Chem. Soc., Dalton Trans.* (1988) 1969.
- [43] See, for example, together with references therein: D. Reed, *Chem. Soc. Rev.* 22 (1993) 109.
- [44] See, for example, together with references therein: J.D. Kennedy, Boron, in: J. Mason (Ed.), *Multinuclear NMR*, Plenum, New York and London, 1987, p. 221 (Chapter 8).

- [45] W. McFarlane, *Proc. Roy. Soc. (London), Ser. A* 306 (1968) 185.
- [46] G.M. Sheldrick, *Acta Crystallogr., Sect. A* 46 (1990) 467.
- [47] G.M. Sheldrick, *SHELX 97, Program System for X-ray Structure Refinement*, University of Göttingen, 1997.
- [48] Z. Otwinowski, W. Minor, *Meth. Enzymol.* 27 (1997) 307.
- [49] COLLECT, Data Collection Strategy Program, Nonius, 1999.
- [50] Z. Otwinowski, W. Minor, SMART, SAINT, SADABS, SHELXTL and APEX2, Bruker AXS Inc., Madison, WI, USA, 1997-2004.
- [51] P. van der Sluis, C.A. Spek, *Acta Crystallogr., Sect. A* 46 (1990) 194.
- [52] R.J. Cernik, W. Clegg, C.R.A. Catlow, G. Bushnell-Wye, J.V. Flaherty, G.N. Greaves, I. Burrows, D.J. Taylor, S.J. Teat, M. Hamichi, *J. Synchrotron Rad.* 4 (1997) 279.
- [53] J. Bould, W. Clegg, J.D. Kennedy, S.J. Teat, M. Thornton-Pett, *J. Chem. Soc., Dalton Trans.* (1997) 2005.
- [54] W. Clegg, M.R.J. Elsegood, S.J. Teat, C. Redshaw, V.C. Gibson, *J. Chem. Soc., Dalton Trans.* (1998) 3037.
- [55] W. Kutzelnigg, M. Schindler, U. Fleischer, *NMR, Basic Principles and Progress*, vol. 23, Springer, Berlin, New York, 1990, p. 165.
- [56] U. Meier, C. van Wüllen, M. Schindler, *J. Comput. Chem.* 13 (1992) 551.
- [57] J.A. Pople et al., *Gaussian 98, Revision A.7*, Gaussian, Inc., Pittsburgh, PA, 1998, and references therein.
- [58] J.A. Pople et al., *Gaussian 03, Revision B.05*, Gaussian, Inc., Pittsburgh, PA, 2003.
- [59] See, for example, together with references therein: J.W. Bausch, A.J. Tebben, Computational studies of nido-C₄B₇H₁₁ carboranes and nido-8-vertex boranes and carboranes, in: J. Casanova (Ed.), *The Borane–Carborane–Carbocation Continuum*, Wiley, New York, NY, 1998, p. 217 (Chapter 9).
- [60] ORTEP3 for Windows, L.J. Farrugia, *J. Appl. Crystallogr.* 30 (1997) 565.
- [61] J. Bould, M. Bown, J.D. Kennedy, *Collect. Czech. Chem. Commun.* 70 (2005) 410.
- [62] J. Bould, T. Jelínek, S.A. Barrett, S.J. Coles, M.J. Hursthouse, M. Thornton-Pett, B. Štíbr, J.D. Kennedy, *Dalton Trans.* (2005) 1499.